Scaling of the Reynolds number in turbulent thermal convection

Chao Sun and Ke-Qing Xia
Department of Physics, The Chinese University of Hong Kong, Shatin, Hong Kong, China
(Received 20 June 2005; published 14 December 2005)

A riddle in turbulent thermal convection is the apparent dispersion from 0.42 to 0.5 in the value of the scaling exponent γ of experimentally measured Reynolds number $\mathrm{Re}\sim\mathrm{Ra}^{\gamma}$, where Ra is the Rayleigh number. The measured Re may be divided into two groups: one based on the circulation frequency of the mean wind and the other based on a directly measured velocity. With new experimental results we show that in frequency measurements the dispersion in γ is a result of the evolution in the circulation path of the wind, and that in the velocity measurements it is caused by the inclusion of a counterflow in the mean velocity. When these factors are properly accounted for both groups give $\gamma=0.5$, which may imply that a single mechanism is driving the flow for both low and high values of Ra.

DOI: 10.1103/PhysRevE.72.067302 PACS number(s): 47.27.Jv, 44.25.+f, 05.65.+b

As a paradigm for the turbulent thermal convection problem, the Rayleigh-Bénard (RB) model contains rich dynamics and organized structures and the understanding of this system will shed light on a wide range of convection phenomena occurring in nature [1–3]. The control parameters in the RB problem are the Rayleigh number $\mathrm{Ra}=\alpha g\Delta T L^3/\nu\kappa$ and the Prandtl number $\mathrm{Pr}=\nu/\kappa$, where ΔT is the temperature difference across a fluid layer of height L, g being the gravitational acceleration, and α, ν, and κ, respectively, the volume expansion coefficient, kinematic viscosity, and thermal diffusivity of the convecting fluid. In a laboratory experiment the fluid is inevitably confined laterally so that the aspect ratio Γ (lateral dimension of the fluid over its height) also enters the problem. Two quantities, the Nusselt number Nu (the dimensionless heat flux) and the Reynolds number Re, represent the global response of the system to the applied thermal driving.

A distinct feature of turbulent thermal convection in a closed box is a large-scale circulatory flow (LSC), also called the mean wind [4]. LSC exists also in the earth's atmosphere, oceans, and core. As the largest flow structure in the system, the wind velocity V_W may be used to define the Reynolds number of the system: $\mathrm{Re}=V_W L/\nu\sim\mathrm{Ra}^{\gamma}$, where Re has been written as a power law of Ra. A riddle exists concerning the scaling exponent γ, namely a large number of experiments have produced a range of its value from 0.42 to 0.5. The difference is large enough that it cannot be explained by experimental uncertainties and differences in the techniques used [5]. Because the properties of Re reflect the underlying driving mechanism and energy budget, this discrepancy is naturally a great cause of concern [6]. It also has implications to other types of buoyancy-driven flows that are ubiquitous in nature. This paper attempts to explain the observed dispersion in γ. As $\Gamma=1$ cell is the most widely used, it will be the configuration discussed here. There exists a large number of Re measurements [7,8] and they may be divided into two groups according to how Re is obtained [5]. In the first one, the circulation frequency f_C of the wind is measured and is then used to obtain Re, which we shall refer to as frequency measurements. In the second one, a velocity is directly measured to obtain Re, which we shall refer to as velocity measurements. We shall see below that there are different reasons for the γ dispersion in the two groups.

Frequency measurement. In this type of experiment f_C is usually identified as the frequency of a prominent peak in either the temperature [5,9–15] or the velocity power spectra [8,13,16,17] measured locally in the convection cell. Using f_C one obtains a Reynolds number $\mathrm{Re}_f=4f_C L^2/\nu$. Sometimes κ is used instead of ν in which case we have the Péclet number $\mathrm{Pe}=\mathrm{RePr}$. The difference being that when Pr is not a constant but varies slightly the use of Pe will minimize the data scatter because of its weak dependence on Pr. For the ease of discussion, we shall hereafter use Re to represent both. We first discuss results from the present work, which will set stage for the discussions that follow. Two water-filled $\Gamma=1$ cylindrical convection cells of respective heights 19.3 and 100 cm are used in the experiment, which have been described in detail in [18,19], respectively. Briefly they consist of copper top and bottom plates and a Plexiglas sidewall. Local temperature is measured by a small thermistor inserted through the sidewall at midheight [20], and data are acquired over periods from 20 to 10 h for low and high Ra, with Ra varied from 10^8 to 10^{12} all at fixed $\mathrm{Pr}=4.3$. From the temperature power spectrum we obtain f_C and then Re_f which is plotted in Fig. 1 as a function of Ra, the solid lines are power law fits to the respective data that give $\mathrm{Re}_f\sim\mathrm{Ra}^{0.45}$ for the 19 cm cell and $\mathrm{Re}_f\sim\mathrm{Ra}^{0.50}$ for 100 cm cell. The inset shows a compensated plot of $\mathrm{Re}_f\mathrm{Ra}^{-1/2}$ (see below for an explanation of the solid triangles). These results show that the measured exponent (denoted as γ_m) is less than 0.5 for small Ra but saturates at 0.5 for $\mathrm{Ra}\gtrsim 10^{11}$.

We now discuss the dispersion in γ_m and its saturation at 0.5. Implicitly contained in Re_f is a relation $V_W=4Lf_C$, in which $4L$ has been taken to be the circulation path length ℓ of the wind ($2L$ or πL is sometimes used instead of $4L$ but this is not critical to our argument here). An important step in understanding the dispersion in γ came from the recognition by Niemela and Sreenivasan (NS) that the circulation path length of the wind is not a constant but evolves with Ra [21]. Indeed, using the measured V_W and f_C, NS obtained an ℓ as a function of Ra and offered an explanation for the shape change of the wind [21]. The evolution of the shape of the wind with Ra was later shown directly by two-dimensional (2D) velocity maps measured using the Particle Image

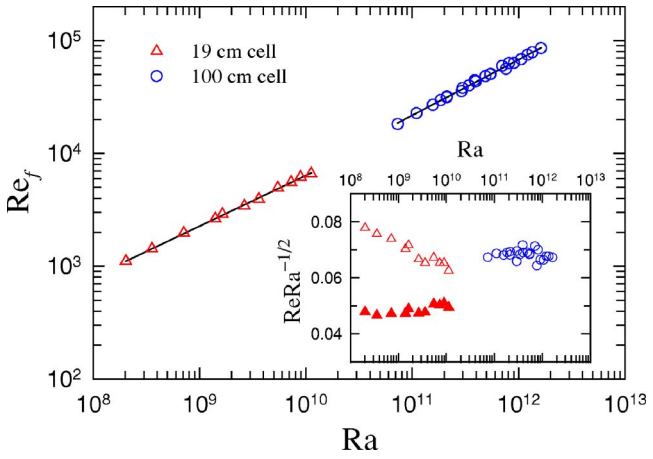

FIG. 1. (Color online) Frequency-based Reynolds number as a function of Ra measured in two cylindrical cells. The lines represent power law fits to the respective data sets (see text). Inset: Re$_f$ (open symbols) and Re$_\ell$ (solid symbols) reduced by Ra$^{1/2}$ vs Ra.

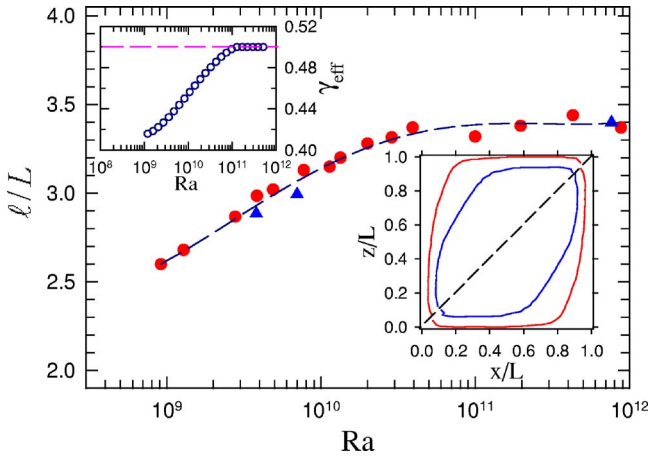

FIG. 2. (Color online) Normalized circulation path length ℓ/L of the wind as a function of Ra, the circles and triangles are from the rectangular and cylindrical cells, respectively. Lower inset: Measured circulation path of the wind for two values of Ra: 3.8×10^9 (inner loop) and 3.5×10^{10} (outer loop). Upper inset: The effective scaling exponent γ_{eff} derived from measured ℓ as a function of Ra.

Velocimetry (PIV) technique [22], which also confirmed the schematic picture shown in [21]. With the path length ℓ now a function of Ra we write $f_C=V_W/\ell$ and Re$_f$ becomes

$$\mathrm{Re}_f=\left(\frac{V_W L}{\nu}\right)\left(\frac{L}{\ell}\right)=\mathrm{Re}\left(\frac{L}{\ell}\right)\sim \mathrm{Ra}^{\gamma_{eff}}, \qquad (1)$$

where, for convenience, we have written $\ell=L\mathrm{Ra}^{\delta}$ and defined $\gamma_{eff}=\gamma-\delta$. It is clear that the exponent γ_m from the measured f_C is just an effective exponent that depends on the circulation path length of the wind; it equals γ when ℓ becomes independent of Ra. It is important to recognize that in writing $f_C=V_W/\ell$ we advance a view that V_W and ℓ are independent quantities while f_C is derived from the two. The wind is a coherent structure of organized thermal plumes that drive the wind and in turn being driven by it in a self-sustained cycle and on average the typical path traversed by the organized (or clustered) plumes is just the mean circulation path of the wind [5,13,18,22,23]. It has been found previously that the wind becomes coherent only above certain critical Ra but thereafter continues to increase its level of coherence with Ra [13]. The shape evolution of the wind is part of this dynamic process of self-organization and synchronization of plume motions. As the plumes rise and/or fall their buoyant potential energy converts into kinetic energy, giving rise to a free-fall velocity $V_{free}=(\alpha g\Delta TL)^{1/2}$. Indeed, as we shall see below, when V_W is properly identified it yields $\gamma=0.5$. That the plume velocity is free-fall type has also been found in a numerical study [24]. Therefore, the properties of f_C reflect both the evolution of the wind via ℓ and the energy balance of the plumes via V_W.

To verify the above argument we need an independently measured ℓ. In a previous study the 2D velocity field in the circulation plane of the wind has been measured using PIV in two rectangular cells over the range of Ra from 9×10^8 to 9×10^{11} at Pr=4.3 [22]. The two cells have $\Gamma=1$ when viewed in the circulation plane of the wind. We define the circulation path-length ℓ as twice of the typical path traversed by the clustered plumes between the two plates. Operationally it is determined as the "particle path" [25] that passes through the points having the maximum velocity in the time-averaged velocity map [22]. Two such paths are shown in the lower inset of Fig. 2, where the path below the diagonal is just a reflection of the one above which is the measured path. By integrating over such paths we obtain ℓ, which are shown in Fig. 2, where circles are from the rectangular cells and triangles are similarly obtained from PIV measurements in the two cylindrical cells. In previous studies [5,13] it has been found that $f_C\approx U/(2L)$, where U is the velocity at midheight of the cell, which implies that $\ell\approx2L$. As the velocity is not a constant along the plumes' path a more accurate determination of ℓ should be the direct integration of the plumes path as is done here. From Fig. 2 it is seen that the measured $\ell\approx2.6L$ for $\mathrm{Ra}\approx10^9$. It should be mentioned that the path length deduced by NS shows a similar trend as our measured ℓ (their definition of ℓ is slightly different than the one used here so that it saturates at a different value [21]). Figure 2 shows that ℓ is not a simple power law for the entire range of Ra. To obtain γ_{eff} we extracted a local exponent δ(Ra) using a polynomial fit of ℓ (dashed line in Fig. 2) for every half decade of Ra between 10^9 and 10^{12}; γ_{eff} is then simply $0.5-\delta$ where $\gamma=0.5$ is used. The upper inset of Fig. 2 shows how γ_{eff} varies with Ra, in particular, the saturation of γ_{eff} at 0.5 for $\mathrm{Ra}\gtrsim10^{11}$ is in excellent agreement with the independently measured Re$_f$ (or f_C) shown in Fig. 1. Indeed, a compensated plot using Re$_f$ from [14] also reveals the saturation of γ_m at 0.5 for $\mathrm{Ra}\gtrsim10^{11}$. Note that Ahlers *et al.* recently also found $\gamma_m=0.5$ at large Ra but the saturation appears to come at a lower Ra [26]. Table I lists the values of γ_m from frequency measurements in the literature that are known to us, along with the range of Ra and Pr of the respective experiments (where there are similar results obtained under similar conditions from the same group, only one is cited). In column five a range of values of γ_{eff} is given which corresponds to the

TABLE I. Scaling exponent γ_m obtained in frequency measurements and γ_{eff} obtained from circulation path lengths of the wind.

Ref.	Ra	Pr	γ_m	γ_{eff}	$\langle\gamma_{eff}\rangle$
[9]	10^8–10^{12}	0.7–1.5	0.49	0.42–0.5	0.46
[11]	10^6–10^8	0.024	0.44±0.02	0.42	0.42
[12]	10^6–10^9	0.025	0.424	0.42–0.44	0.42
[16]	10^{12}–10^{14}	27–190	0.43±0.02	0.5	0.5
[13]	10^8–10^{10}	5.4	0.46	0.42–0.46	0.44
[14]	10^6–10^{13}	0.7	0.47	0.42–0.5	0.46
[17]	10^8–10^{10}	3–1200	0.43	0.42–0.46	0.44
[15]	10^8–10^9	6.0	0.46±0.01	0.42–0.43	0.42
Present	10^8–10^{10}	4.3	0.45	0.42–0.46	0.44
Present	10^{11}–10^{12}	4.3	0.50	0.5	0.5

range of Ra varied in the respective experiments. In calculating γ_{eff}, a value of 0.5 is assigned if the lowest Ra in the corresponding experiment is larger than $\mathrm{Ra}=10^{11}$ and a value of 0.42 is assigned if the highest Ra is less than 10^9. It is seen that most of the measured γ_m fall into the range of γ_{eff} determined from the circulation path. Column six gives $\langle\gamma_{eff}\rangle$, which is a simple average of γ_{eff} over the range of Ra varied in the corresponding experiment. It is seen that the agreement between $\langle\gamma_{eff}\rangle$ and γ_m is remarkable, especially when considering the fact that in some of the experiments data points are not uniformly distributed in Ra whereas in calculating $\langle\gamma_{eff}\rangle$ every half decade of Ra has been given equal weight. Another way of verifying our result is to obtain the Reynolds number using the independently measured ℓ and f_C, i.e., $\mathrm{Re}_\ell=\ell f_C L/\nu$. The solid triangles in the inset of Fig. 1 represent $\mathrm{Re}_\ell \mathrm{Ra}^{-1/2}$ (data from the 19 cm cell); this shows that the deviation of f_C (or Re_f) from $\gamma=0.5$ is now compensated by an opposite change in ℓ to yield an exponent of 0.5 (note that the magnitudes of Re_ℓ and Re_f are not expected to be the same because "4" is incorrectly used in Re_f). An important point to note is that the measured f_C is insensitive to the position of the measuring probe in the convection cell. This fact has been found in a previous measurement of local velocity [27] and temperature [28] at varying distances from the sidewall. The reason is that although the circulation frequency of the wind is determined by the traveling path of the organized plumes, the motion of the plumes generate an oscillation of the same frequency in the bulk fluid which can be detected in most parts of the convection cell [5,18,29]. Also, to be noted is that the present ℓ is measured with $10^9 \leqslant \mathrm{Ra} \leqslant 10^{12}$ and Pr=4.3, while these parameters vary over a much wider range in the experiments cited in Table I. For Ra the problem may not be a severe one, as the present ℓ is not far from $2L$ which may be taken as a safe lower bound. In addition to the likely case of ℓ being a function of Pr, as far as γ is concerned the more relevant question here is whether the Ra dependence of ℓ depends on Pr, which remains to be explored. The point here is we should refrain from making too detailed a comparison with the specific results listed in the table because of all these uncertainties. Rather we should take an overall view, which is, despite all the limitations, our explanation has largely accounted for most of the dispersions

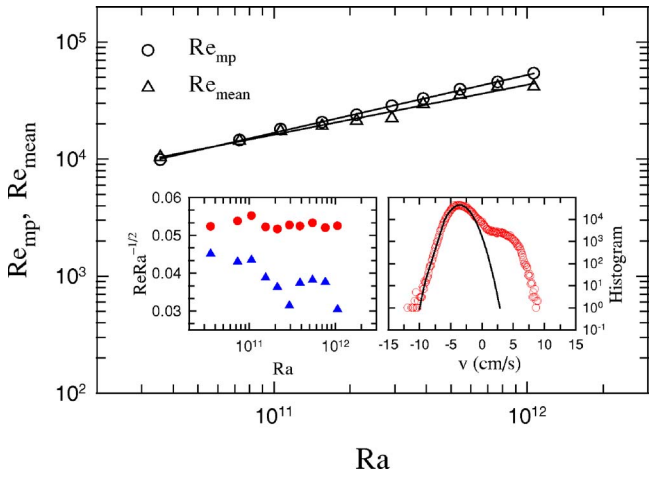

FIG. 3. (Color online) Reynolds number Re_{mp} and Re_{mean} vs Ra. Left inset: Compensated plot of $\mathrm{Re}_{mp}\mathrm{Ra}^{-1/2}$ (circles) and $\mathrm{Re}_{mean}\mathrm{Ra}^{-1/2}$ (triangles) vs Ra (for clarity, $\mathrm{Re}_{mean}\mathrm{Ra}^{-1/2}$ has been shifted down by 0.01). Right inset: Histogram of the local velocity measured at $\mathrm{Ra}=1.1\times10^{12}$.

in γ_m from the frequency measurements reported in the literature.

Velocity measurement. In this type of measurement, an absolute velocity is obtained using either two temperature probes or two laser beams, or standard velocimetry techniques such as Laser Doppler Velocimetry (LDV) [8,10,13,14,29–34]. A review of the various methods can be found in [8]. We first discuss results from the present work, which are obtained in the 100 cm cell using the LDV method. Local velocity is measured at a position 5 cm from the sidewall in the circulation plane of the wind at midheight, with varying Ra and fixed Pr=4.3, for durations ranging from 10 to 24 h. The right inset of Fig. 3 shows a histogram of the vertical velocity, where the solid line is a fit of Gaussian function to the main peak of the histogram. In addition to the large peak located at $V\approx-3.6$ cm/s a small peak can be seen appearing at $V\approx+3.6$ cm/s. Such a peak arises from either the occasional change in the circulation direction of the wind [14,35–37] or energetic plumes traveling along the sidewall but in the "wrong" direction [22]. In a tilted cell the overall change in the wind's circulation direction is suppressed, so that only the second source contributes to the small peak, which has indeed been observed in previous velocity measurements with tilted cells [8,29]. We call this occasional flow in the opposite direction to the mean flow, the counterflow, regardless of its cause. It is clear that counterflows reduce the average velocity and change the characteristic magnitude of the circulation speed of the wind. In fact, when flows in either direction become equally probable, as is the case when Ra becomes very large [14], the mean velocity will be close to zero. This means that a properly chosen wind velocity V_W should not include the counterflow. Since without the counterflow the velocity distribution is Gaussian, we can use the most probable velocity V_{mp} as V_W. Figure 3 plots two Reynolds numbers $\mathrm{Re}_{mp}=V_{mp}L/\nu$ and $\mathrm{Re}_{mean}=V_{mean}L/\nu$ vs Ra, where the solid lines represent power law fittings to the respective data: $\mathrm{Re}_{mp}=0.06\mathrm{Ra}^{0.50\pm0.01}$ and $\mathrm{Re}_{mean}=0.33\mathrm{Ra}^{0.43\pm0.02}$, where V_{mean} is a simple average of

the measured velocity. The left inset is a compensated plot of $\mathrm{Re}_{mp}\mathrm{Ra}^{-1/2}$ and $\mathrm{Re}_{mean}\mathrm{Ra}^{-1/2}$ vs Ra. It is clear that the use of V_{mean} reduces γ and $\gamma=0.5$ if V_{mp} is used. Because the counterflow is a rare and stochastic event, its contribution to the measured velocity will fluctuate unless sufficiently long data averaging is made, which is probably why Re_{mean} is more scattered than Re_{mp} in Fig. 3. We now examine results from the literature under this light. A check of the literature shows that experiments that effectively used V_{mp} for Re all gave $\gamma=0.5$ [14,31,33], whereas experiments that effectively used V_{mean} for Re produced a γ that varies from 0.43 to 0.49 [8,10,13,29,30,32,34]. The deviation from 0.5 in the latter group varies probably because the contribution to V_{mean} from the counterflow varies with both Ra and the averaging time of the measurements. Note that in the dual-laser-beam method used in [31,33], either $+v$ or $-v$ was measured but not both so that the average velocity obtained in those experiments is just V_{mp} defined here. On the other hand, in the dual-temperature-probe method an average would give V_{mean}. Thus it appears that if a proper V_W is used then Re will have a scaling exponent of 0.5. With the wind velocity properly identified, a consistency check may be made. As shown in Fig. 2, the circulation pathlength ℓ saturates to a value $\ell_0 \approx 3.4L$ for $\mathrm{Ra} \gtrsim 10^{11}$. Using f_C measured in the 100 cm cell and the above V_{mp} we find that indeed $V_{mp} \approx f_C \ell_0$ for the entire range of Ra from 7.3×10^{10} to 1.6×10^{12}.

In summary, we have in this paper offered possible causes for the observed dispersion in the scaling exponent γ of the Reynolds number Re with the Rayleigh number Ra measured in a large number of turbulent thermal convection experiments. Moreover, the global Reynolds number appears to be dictated by a free-fall velocity which gives $\gamma=0.5$. Finally we remark that the explanations we give here should be equally applicable to numerical experiments for both groups of measurements [24,38]. A question for future experiments is how ℓ varies with Pr, which will affect the Pr scaling of Re obtained from frequency measurements.

This work was supported by the Hong Kong Research Grants Council (Project No. CUHK403003).

[1] E. Siggia, Annu. Rev. Fluid Mech. **26**, 137 (1994).
[2] S. Grossmann and D. Lohse, J. Fluid Mech. **407**, 27 (2000).
[3] L. Kadanoff, Phys. Today **54**(8), 34 (2001).
[4] R. Krishnamurti and L. N. Howard, Proc. Natl. Acad. Sci. U.S.A. **78**, 1981 (1981).
[5] X.-L. Qiu and P. Tong, Phys. Rev. E **66**, 026308 (2002).
[6] S. Grossmann and D. Lohse, Phys. Rev. E **66**, 016305 (2002).
[7] X. Chavanne, F. Chillà, B. Chabaud, B. Castaing, and B. Hébral, Phys. Fluids **13**, 1300 (2001).
[8] X.-L. Qiu and P. Tong, Phys. Rev. E **64**, 036304 (2001).
[9] B. Castaing *et al.*, J. Fluid Mech. **204**, 1 (1989).
[10] T. Takeshita, T. Segawa, J. A. Glazier, and M. Sano, Phys. Rev. Lett. **76**, 1465 (1996).
[11] A. Naert, T. Segawa, and M. Sano, Phys. Rev. E **56**, R1302 (1997).
[12] S. Cioni, S. Ciliberto, and J. Sommeria, J. Fluid Mech. **335**, 111 (1997).
[13] X.-L. Qiu and P. Tong, Phys. Rev. Lett. **87**, 094501 (2001).
[14] J. J. Niemela, L. Skrbek, K. R. Sreenivasan, and R. J. Donnelly, J. Fluid Mech. **449**, 169 (2001).
[15] D. Funfschilling and G. Ahlers, Phys. Rev. Lett. **92**, 194502 (2004).
[16] S. Ashkenazi and V. Steinberg, Phys. Rev. Lett. **83**, 3641 (1999).
[17] S. Lam, X.-D. Shang, S.-Q. Zhou, and K.-Q. Xia, Phys. Rev. E **65**, 066306 (2002).
[18] C. Sun, K.-Q. Xia, and P. Tong, Phys. Rev. E **72**, 026302 (2005).
[19] C. Sun, L.-Y. Ren, H. Song, and K.-Q. Xia, J. Fluid Mech. **542**, 165 (2005).
[20] S.-Q. Zhou and K.-Q. Xia, Phys. Rev. Lett. **87**, 064501 (2001).
[21] J. J. Niemela and K. R. Sreenivasan, Europhys. Lett. **62**, 829 (2003).
[22] K.-Q. Xia, C. Sun, and S.-Q. Zhou, Phys. Rev. E **68**, 066303 (2003).
[23] H.-D. Xi, S. Lam, and K.-Q. Xia, J. Fluid Mech. **503**, 47 (2004).
[24] R. M. Kerr, Phys. Rev. Lett. **87**, 244502 (2001).
[25] See, for example, D. J. Tritton, *Physical Fluid Dynamics*, 2nd ed. (Clarendon Press, Oxford, 1988). The software TecPlot is used to determine the particle path.
[26] G. Ahlers, E. Brown, and A. Nikolaenko (unpublished).
[27] X.-D. Shang and K.-Q. Xia, Phys. Rev. E **64**, 065301(R) (2001).
[28] S.-Q. Zhou, C. Sun, and K.-Q. Xia (unpublished).
[29] X.-L. Qiu, X.-D. Shang, P. Tong, and K.-Q. Xia, Phys. Fluids **16**, 412 (2004).
[30] M. Sano, X.-Z. Wu, and A. Libchaber, Phys. Rev. A **40**, 6421 (1989).
[31] Y.-B. Xin, K.-Q. Xia, and P. Tong, Phys. Rev. Lett. **77**, 1266 (1996).
[32] X. Chavanne, F. Chillà, B. Castaing, B. Hébral, B. Chabaud, and J. Chaussy, Phys. Rev. Lett. **79**, 3648 (1997).
[33] X.-L. Qiu and K.-Q. Xia, Phys. Rev. E **58**, 486 (1998).
[34] X.-L. Qiu, S.-H. Yao, and P. Tong, Phys. Rev. E **61**, R6075 (2000).
[35] E. Brown, A. Nikolaenko, and G. Ahlers, Phys. Rev. Lett. **95**, 084503 (2005).
[36] F. F. Araujo, S. Grossmann, and D. Lohse, Phys. Rev. Lett. **95**, 084502 (2005).
[37] H.-D. Xi, Q. Zhou, and K.-Q. Xia (unpublished).
[38] R. Verzicco and R. Camussi, J. Fluid Mech. **383**, 55 (1999).